Quasi-classical trajectory study of the reaction H′ + HS on a new ab initio potential energy surface H2S (3A″)

8 AUTHORS, INCLUDING:

Zou Jinghan
Dalian Institute of Chemical Physics
3 PUBLICATIONS **1** CITATION

SEE PROFILE

Shuhui Yin
Dalian Maritime University
15 PUBLICATIONS **35** CITATIONS

SEE PROFILE

Wu Dan
Dalian Maritime University
3 PUBLICATIONS **1** CITATION

SEE PROFILE

Hong Gao
Dalian Maritime University
18 PUBLICATIONS **16** CITATIONS

SEE PROFILE

Quasi-classical trajectory study of the reaction H′ + HS on a new *ab initio* potential energy surface H₂S (^{3}A″)

JINGHAN ZOU[a], SHUHUI YIN[a,*], DAN WU[a], MINGXING GUO[b], XUESONG XU[a], HONG GAO[a], LEI LI[a] and LI CHE[a]

[a]Department of Physics, Dalian Maritime University, Dalian 116026, China
[b]Environmental Science and Engineering College, Dalian Maritime University, Dalian 116026, Liaoning, China
e-mail: yinsh@dlmu.edu.cn

Abstract. Theoretical study on the dynamics of reactions H′ + HS($v = 0, j = 0$)→H₂ + S and H′ + HS($v = 0, j = 0$)→H + H′S is performed with quasi-classical trajectory (QCT) method on a new *ab initio* potential energy surface for the lowest triplet state of H₂S (^{3}A″) constructed in 2012 by Lv *et al*. The QCT-calculated reaction integral cross-sections are in good agreement with previous quantum wave packet results over the collision energy range of 0–50 kcal/mol. Both the abstraction and exchange reactions are governed by direct reaction dynamics and the trajectories follow the minimum energy path. The rotational angular momentum vector j' of products in the two reaction channels are not only aligned perpendicular to scattering plane but also oriented along the negative direction of the axis perpendicular to the scattering plane. With the increase in collision energy, the variation trends of product polarization in the two reaction channels are different and that may be attributed to the obviously different characteristic of the two channels on the potential energy surface.

Keywords. Reaction stereodynamics; quasi-classical trajectory; cross-section; polarization.

1. Introduction

In recent decades, the chemical reaction S + H₂ and its variants have attracted abundant attention, in both experimental and theoretical aspects, for its important role in combustion and atmospheric chemistry.[1–19] Lee and Liu applied a crossed molecular beam apparatus method to map out the differential cross-section (DCS) of the reactions.[15,17] The DCSs peaked in both the forward and backward directions with some preference towards the forward direction, implying a long-lived H₂S reaction intermediate. This is also supported by experimental total integral cross-sections (ICS) that decay monotonically with the increase in collision energy.[16] Recently, with the advent of experimental techniques that allow the cooling of translational degrees of freedom, Berteloite *et al*.[18] performed kinetics and crossed-beam experiments to measure absolute rate coefficients down to 5.8 K and relative integral cross-sections to collision energies as low as 0.68 meV. Theoretically, earlier studies include a statistical model study[1] of the reactions S(^{1}D) + H₂, HD, D₂ based on the Rice–Ramsperger–Kassel–Marcus

(RRKM) theory. Zyubin *et al*.[3] carried out extensive multireference configuration interaction (MRCI) *ab initio* calculations with multiconfiguration self-consistent field (MCSCF) reference wavefunctions for all the potential energy surfaces (PESs) that correlate with the reagents. Subsequently, an improved version of the 1^{1}A′ PES (RKHS PES) based on the same *ab initio* points was produced by Ho *et al*.[4] with the reproducing kernel Hilbert space (RKHS) interpolation method. This PES has been extensively used in quasi-classical trajectory (QCT),[4–7] time-independent quantum mechanical (TI-QM),[6,8] wave packet (WP)[12,20,21] rigorous statistical quantum mechanical (SQM)[9,11,22] and statistical quasi-classical trajectory (SQCT)[10] dynamical calculations. Song and Varandas[23] calculated a new *ab initio* PES (DMBE/CBS PES) by fitting accurate multireference configuration interaction energies with large basis sets and extrapolation to the complete basis set limit.[24] More recently, Lara *et al*. calculated reaction probability as a function of total angular momentum and reaction cross-section for the collision of open shell S (^{1}D) atoms with para-hydrogen over the kinetic energy range of 0.09–10 meV based on both RKHS PES and DMBE/CBS PES.[19] The results revealed very different dynamical behaviours on the two PESs at low collision energies.

Most of the studies mentioned here have focused on the insertion reaction S + H$_2$, while the reverse reaction H′ + HS attracts our interest. The reaction H′ + HS is a prototype for hydrogen-atom abstraction and exchange reactions and can provide important information in dynamic studies. There are several PESs for the reverse reaction H′ + HS [13,14,25] from previous studies. In 2012, Lv *et al.* constructed a new *ab initio* PES for the lowest triplet state of H$_2$S (^{3}A″). [26] On this new PES, the total reaction probabilities were calculated by the time-dependent wave packet (TDWP) and QCT methods and the integral cross-sections were obtained by TDWP method over the collision energy (E_{col}) range of 0.0–2.0 eV for the reactant HS initially at the ground and the first vibrationally excited states. As far as we know, there is seldom investigation on the reaction H′ + HS, especially on its stereodynamics. To shed more light on this reverse reaction, in this study we will adopt a QCT calculation on the new PES constructed by Lv *et al.* [26]

2. Theory

2.1 *Rotational polarization of the product*

Figure 1 is the centre of mass (CM) frame, which is employed in the present calculation. The full three-dimensional angular distribution related k–k'–j' can
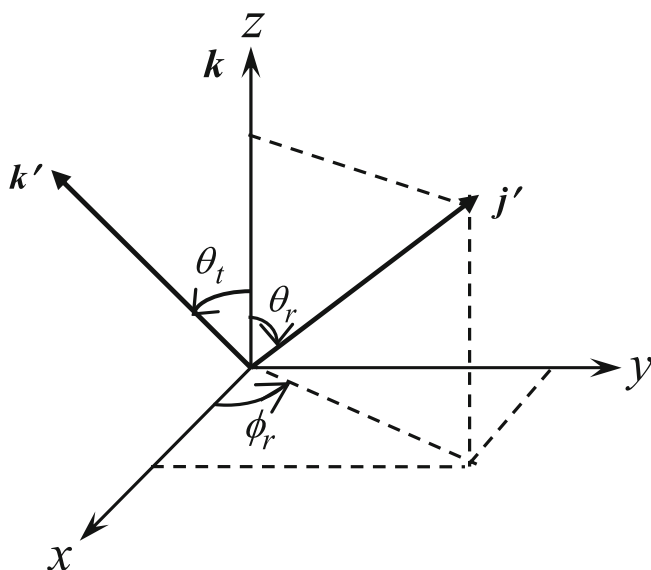

Figure 1. Centre-of-mass frame used to describe the k, k', j' correlations. The z-axis of CM frame is parallel to the reagent initial relative velocity vector k, while the zx-plane (the scattering plane) contains k and k' (the product final relative velocity vector) and the y-axis is the axis perpendicular to the scattering plane.

be represented by a set of generalized polarization-dependent differential cross-sections (PDDCSs) of the CM frame. The z-axis of CM frame is parallel to the reagent initial relative velocity vector k, while the zx-plane (the scattering plane) contains k and k' (the product final relative velocity vector) and the y-axis is the axis perpendicular to the scattering plane. The angle θ_t is the so-called scattering angle between the reagent relative velocity and the product relative velocity. θ_r and ϕ_r are the polar and azimuthal angles of the final rotational angular momentum j'. The fully correlated CM angular distribution is written as the sum [27]

$$P(\omega_t, \omega_r) = \sum_{kq} \frac{2k+1}{4\pi} \frac{1}{\sigma} \frac{d\sigma_{kq}}{d\omega_t} C_{kq}(\theta_r, \phi_r)^*, \quad (1)$$

where $-k \leq q \leq k$, $(1/\sigma)(d\sigma_{kq}/d\omega_t)$ are the generalized PDDCSs, [28] and $C_{kq}(\theta_r, \phi_r)$ are modified spherical harmonics [29] and $\frac{1}{\sigma}\frac{d\sigma_{k0}}{d\omega_t}$ yields

$$\frac{1}{\sigma} \frac{d\sigma_{k0}}{d\omega_t} = 0 \quad (k \text{ is odd}), \quad (2)$$

$$\frac{1}{\sigma} \frac{d\sigma_{kq+}}{d\omega_t} = \frac{1}{\sigma} \frac{d\sigma_{kq}}{d\omega_t} + \frac{1}{\sigma} \frac{d\sigma_{k-q}}{d\omega_t} = 0$$
$$(k \text{ even}, q \text{ odd or}, k \text{ odd}, q \text{ even}) \quad (3)$$

$$\frac{1}{\sigma} \frac{d\sigma_{kq-}}{d\omega_t} = \frac{1}{\sigma} \frac{d\sigma_{kq}}{d\omega_t} - \frac{1}{\sigma} \frac{d\sigma_{k-q}}{d\omega_t} = 0$$
$$(k \text{ even}, q \text{ even or}, k \text{ odd}, q \text{ odd}). \quad (4)$$

The PDDCS is written in the following form:

$$\frac{1}{\sigma} \frac{d\sigma_{kq\pm}}{d\omega_t} = \sum_{k_1} \frac{[k_1]}{4\pi} S_{kq\pm}^{k_1} C_{k_1 - q}(\theta_t, 0), \quad (5)$$

where $S_{kq\pm}^{k_1}$ is evaluated using the expected value expression

$$S_{kq\pm}^{k_1} = \langle C_{k_1 q}(\theta_t, 0) C_{kq}(\theta_r, 0)[(-1)^q e^{iq\phi_r} \pm e^{-iq\phi_r}] \rangle, \quad (6)$$

with the angular brackets representing an average over all angles. The differential cross-section is given by

$$\frac{1}{\sigma} \frac{d\sigma_{00}}{d\omega_t} \equiv P(\omega_t) = \frac{1}{4\pi} [k_1] h_0^{k_1}(k_1, 0) P_{k_1}(\cos \theta_t). \quad (7)$$

The bipolar moments $h_0^{k_1}(k_1, 0)$ are evaluated using the expectation values of the Legender moments of the usual differential cross-section:

$$h_0^{k_1}(k_1, 0) = \langle P_{k_1}(\cos \theta_t) \rangle. \quad (8)$$

During the calculations, the truncated number in this expansion is $k_1 = 7$. The distribution function $P(\theta_r)$,

the most common vector correlation, describing the **k**–**j**′ correlation, is expanded in a series of Legendre polynomials[30]

$$P(\theta_r) = \frac{1}{2} \sum_k (2k+1) a_0^{(k)} P_k(\cos\theta_r), \qquad (9)$$

where

$$a_0^{(k)} = \int_0^\pi P(\theta_r) P_k(\cos\theta_r) \sin\theta_r d\theta_r = \langle P_k(\cos\theta_r)\rangle, \qquad (10)$$

with the expansion coefficients $a_0^{(k)}$ referred to as an orientation (k is odd) or alignment (k is even) parameters, and $k = 2$ indicates the product rotational alignment:

$$a_0^2 = \langle P_2(\cos\theta_r)\rangle = \langle P_2(\mathbf{j}' \cdot \mathbf{k})\rangle = \frac{1}{2}\langle 3\cos^2\theta_r - 1\rangle. \quad (11)$$

In this study, we only calculate the average rotational alignment of the product, because it has been measured in most experiments. In the calculations, $P(\theta_r)$ is expanded up to $k = 18$, which shows good convergence. The dihedral angle distribution function $P(\phi_r)$, describing the **k**–**k**′–**j**′ correlation, can be expanded in the Fourier series as

$$P(\phi_r) = \frac{1}{2\pi}\left(1 + \sum_{even,n\geq 2} a_n \cos(n\phi_r)\right.$$
$$\left. + \sum_{odd,n\geq 1} b_n \sin(n\phi_r)\right), \qquad (12)$$

where

$$a_n = 2\langle\cos(n\phi_r)\rangle, \qquad (13)$$

$$b_n = 2\langle\sin(n\phi_r)\rangle. \qquad (14)$$

In this calculation, $P(\phi_r)$ is expanded up to $n = 24$, which is sufficient for good convergence.

2.2 Potential energy surface

In the present calculations, we use a new triplet adiabatic PES constructed by Lv *et al.*[26] The reaction H (^{2}S) + HS ($^2\Pi$) correlates to the singlet states of H_2S (^{1}A′, ^{1}A″) and the triplet states of H_2S (3A′, 3A″). On the lowest adiabatic state H_2S (3A″), the reaction can proceed through an abstraction H′ + HS→H_2 + S and an exchange pathway H′ + HS→H + H′S. The new PES was computed using complete active space self-consistent field (CASSCF)[31,32] and internally contracted MRCI wave function[33–35] with an aug-cc-pV5Z basis set of Dunning.[36] The multireference Davison correction[37] (+Q) was included to compensate for the

effect of higher order correlation. Analytical representation of the PES was fitted with 6600 *ab initio* energies below 3.8 eV relative to the dissociation limit of H–H–S. Analytical PES was generated by the many-body expansion in the Aguado–Paniagua function.[38] Finally, the globally smooth PES was constructed using the procedure described by Aguado *et al.*[39] Compared to the *ab initio* data, the three-body term rms error was 0.43 kcal/mol and the maximum energy deviation was 3.25 kcal/mol. On the PES, there is no potential well and the minimum energy path of the abstraction and exchange reactive processes occur at the collinear configuration of the three nuclei. Moreover, the barrier height increases when the S–H–H and H–S–H bond angles decrease from 180° to 60°. The transition state for the abstraction reaction is found to be linear with $r_{HH} = 2.54\, a_0$ and $r_{HS} = 2.62\, a_0$ (Bohr radius, $1\, a_0 = 5.29177 \times 10^{-11}$ m) and the barrier height is 2.07 kcal/mol with respect to the reactant H + HS asymptote, while the exchange reaction barrier is 7.15 kcal/mol and the transition state lies at linear geometry with $r_{HS} = r_{H'S} = 2.87\, a_0$.

2.3 QCT calculations

We employed the standard QCT method (see the details in Refs [4–7] and the references therein) to study the stereodynamics of the title reactions. The classical Hamilton's equations are numerically integrated in three dimensions. For reaction A + BC, Hamilton equation can be presented by nine coordinate variables (q_1, q_2, q_3), (q_4, q_5, q_6), (q_7, q_8, q_9) and nine conjugated momentum variables (p_1, p_2, p_3), (p_4, p_5, p_6), (p_7, p_8, p_9).

$$\frac{\partial H}{\partial P_i} = \dot{q}_i \quad i = 1, 2, \ldots, 9 \qquad (15)$$

$$\frac{\partial H}{\partial q_i} = -\dot{p}_i \qquad (16)$$

$$H = \frac{1}{2m_A}\sum_{i=1}^3 p_i^2 + \frac{1}{2m_B}\sum_{i=4}^6 p_i^2 + \frac{1}{2m_C}\sum_{i=7}^9 p_i^2$$
$$+ U(q_1, q_2, \ldots q_9). \qquad (17)$$

When there is no external field, Hamilton equation can be decomposed into two parts, centre of mass movement $H_{c.w.}$ and relative movement H_{rel}. The motion of the centre of mass stays the same, and the expression of relative motion H_{rel} can be expressed as:

$$H_{rel} = \frac{1}{2\mu_{BC}}\sum_{j=1}^3 P_j^2 + \frac{1}{2\mu_{A,BC}}\sum_{j=4}^6 P_j^2 + U(r_1, r_2, r_3), \qquad (18)$$

where P_j is conjugated momentum relative to generalized coordinates Q_j, U represents the potential energy function

$$\mu_{BC} = \frac{m_B m_C}{m_B + m_C}, \tag{19}$$

$$\mu_{A,BC} = \frac{m_A(m_B + m_C)}{m_A + m_B + m_C}. \tag{20}$$

The detailed information of the Hamilton equation can be found in ref. 40. The accuracy of the calculation is verified by checking the conservation of total energy and total angular momentum for every trajectory. The vibrational and rotational levels of HS were taken as $v = 0$ and $j = 0$, respectively. Due to $\vec{J} = \vec{L} + \vec{j}$, where $\vec{J}$ and $\vec{L}$ are the total angular momentum and total orbital angular momentum of A + BC system, respectively, in the case of rotational angular momentum of BC $\vec{j} = 0$, we have $\vec{J} = \vec{L}$, which means the scattering plane coincides with the initial molecular plane. In this calculation, batches of 100000 trajectories were run for each reaction and integration step size is chosen as 0.1 fs. The trajectories were started at an initial distance of 10 Å between the H atom and the centre of the mass of the HS molecule.

3. Results and discussion

In figure 2, we compare the integral cross-sections obtained by summing the state-to-state reaction cross-sections, that is, the vibrationally-summed cross-sections, with the results of TDWP in ref. 26 for H′ + HS ($v = 0$, $j = 0$) reactions. It is clear from figure 2. that the QCT and TDWP results for both abstraction and exchange reaction channels are in good agreement, indicating that the quantum effects are not significant in the two reactions and the QCT method is reliable in the title reactions. The integral cross-sections dependent of collision energy for the two reaction channels are remarkably different. For the abstraction reaction H′ + HS($v = 0$, $j = 0$)→H$_2$ + S, the cross-section displays a rapid rise firstly and reaches a plateau, and then declines gradually with the increase in collision energy. For the exchange reaction H′ + HS($v = 0$, $j = 0$)→H + H′S, the cross-section increases steadily to a large value with the increase in collision energy. In addition, the threshold of the abstraction reaction is lower than the exchange reaction. This is due to the different barrier heights on the PES for the two reaction channels. From the new PES of Lv et al.,[26] the barrier height of abstraction reaction is 0.09 eV, while it is 0.31 eV for the exchange reaction. The well-known handicap of QCT method is its inability to properly treat the quantum zero-point energy,[41–47] and
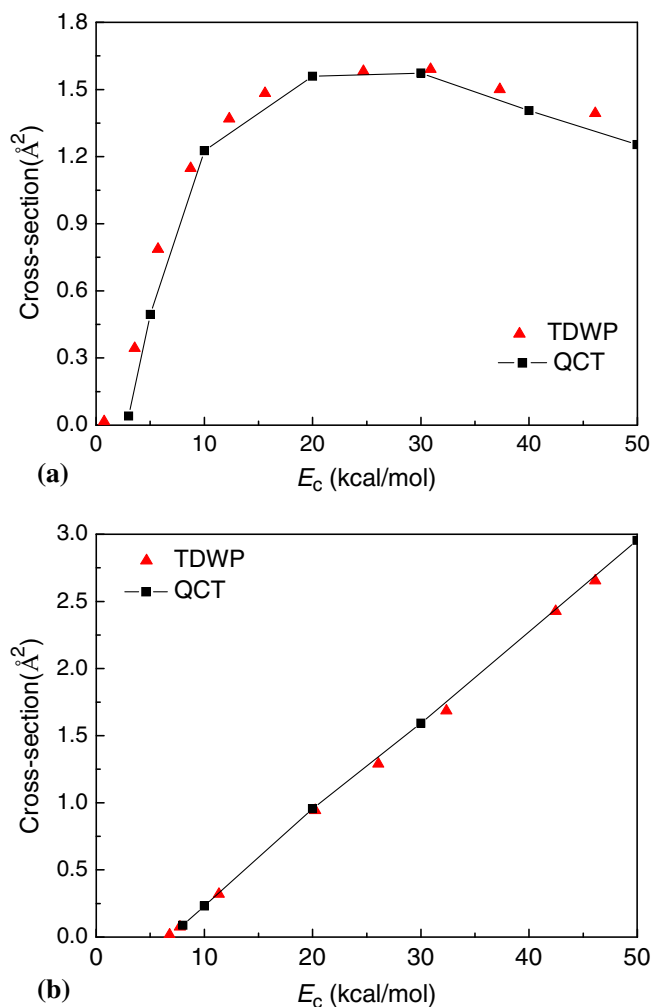

Figure 2. A comparison between the QCT-computed reaction integral cross-section in this study and TDWP result calculated by Lv *et al.*[26] for (**a**) the abstraction reaction H′ + HS($v = 0$, $j = 0$)→H$_2$ + S, and (**b**) the exchange reaction H′ + HS($v = 0$, $j = 0$)→H + H′S.

some methods have been suggested to 'quantize' the continuous vibrational–rotational energy distributions obtained from QCT calculations.[48–50] Recently, Czakó *et al.* implemented some previously suggested methods to avoid zero-point energy leakage and applied it to water dimmer.[51,52] The good agreement between our QCT calculated cross-sections with the TDWP results even near the reaction threshold as shown in figure 2 suggests that the quantum effect is not obvious in the title reactions and the zero-point energy leakage is not a major concern in the present study.

Energy dependence of the integral cross-section for the hydrogen abstraction reaction H′ + HS($v = 0$, $j = 0$)→H$_2$ + S that first rises and then falls as the collision energy increases far over the reaction barrier is essentially similar to the observations in reactions H + HCl,[53] H + HBr[54] and H + CD$_4$.[55] Zhang and Yang

presented that in these hydrogen abstraction reactions, all the reactive events occur through a tug-of-war between the incoming H atom and non-reacting group.[55] From this tug-of-war mechanism, for the abstraction reaction H′ + HS($v = 0$, $j = 0$)→H$_2$ + S, the incoming H′ atom, with collision energy well above the energy barrier, is always reflected in a collision by the repulsive wall at the 'interaction' end of the reaction valley, because the mass of the non-reacting HS group is considerably larger than that of the incoming H′ atom. Only when the H atom happens to depart from the HS group quickly enough, at the time the incoming H′ atom is reflected, does the reflection lead to a reaction. At even higher collision energy, the incoming H′ atom moves too fast after the reflection for the H atom in HS group to catch up. As a result, the reaction probability declines with increase of collision energy. Excess collision energy can only increase the chance for the incoming H′ atom to lose in the tug-of-war mechanism. This tug-of-war mechanism is not involved in the exchange reaction H′ + HS($v = 0$, $j = 0$)→H + H′S. As a direct reaction with a barrier, higher and higher collision energies above the barrier would mean that more and more of the collisions can surmount the energy barrier to reaction. That is the reason for the integral cross-section of the exchange reaction H′ + HS($v = 0$, $j = 0$)→H + H′S showing a monotonic increase with the increase in collision energy.

The calculated distributions of $(2\pi/\sigma)\,(d\sigma_{00}/d\omega_t)$ are shown in figure 3, which is just the DCS distribution, only describes the $\boldsymbol{k}$–$\boldsymbol{k}'$ correction and is not associated with orientation and alignment of final rotational angular momentum $\boldsymbol{j}'$. The DCSs reported in this study are also vibrationally-summed. From figure 3 (a) and (b), the scattering directions of products are greatly different in the two reaction channels. For the abstraction reaction, the DCS shows backward distribution at the low collision energy of 10 kcal/mol. With the increase in collision energy, angular distributions show a substantial decrease of backward distribution together with a shift to sideways when collision energy increase from 10 to 30 kcal/mol, and the backward scattering eventually vanishes with the further increase in collision energy to 50 kcal/mol. In contrast, the products are mainly backward scattered in the exchange reaction channel and the degree of backward scattering declines with the increase in collision energy. To study why these DCSs differ at different collision energies, the variations of internuclear distances are presented as a function of propagation time in figures 4 and 5. From the figures, the attacking H′ atom collides with the HS molecule and forms a H$_2$ or H′S product
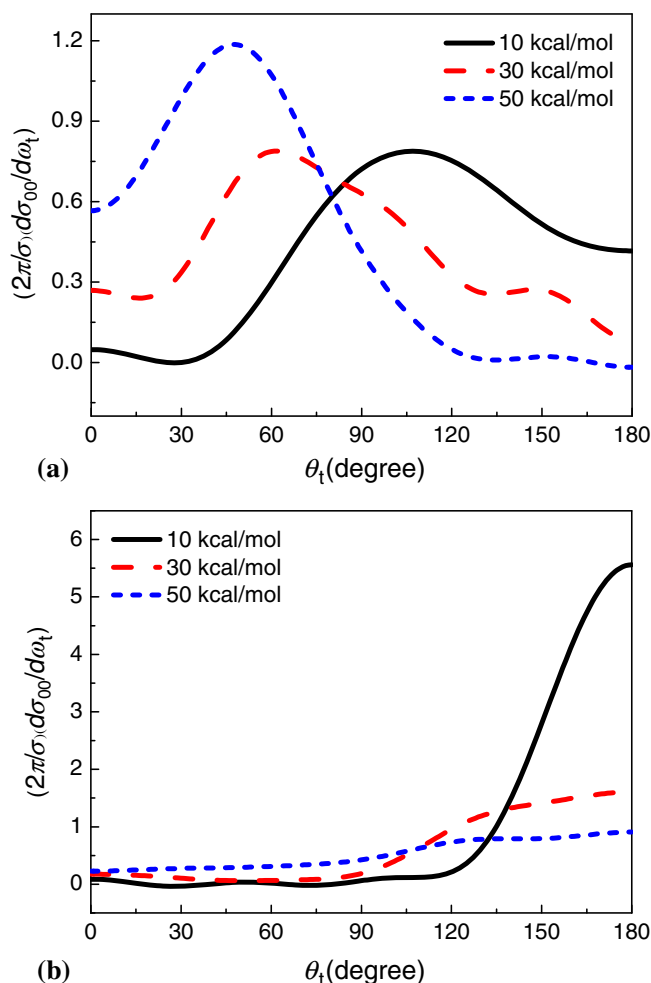

Figure 3. Differential cross-section for (**a**) the abstraction reaction H′ + HS($v = 0$, $j = 0$)→H$_2$ + S, and (**b**) the exchange reaction H′ + HS($v = 0$, $j = 0$)→H + H′S, respectively, plotted as a function of scattering angle.

molecule that immediately recoils. This is consistent with the direct reactive mechanism. These trajectories obey direct reaction and stay near the minimum energy reaction path. It is interesting to find that in the two reaction channels, the scattering direction of product molecules presents different variation tendencies with the increase in collision energy. This phenomenon can be attributed to the different mass combinations and will be discussed in detail here. According to a previous theory,[56] the abstraction reaction channel belongs to a light–light–heavy (LLH) mass combination. The attacking H′ atom abstracts an H atom from the reagent molecule HS and produces the H$_2$ molecule. At low collision energies, the light H$_2$ product with small momentum can recoil easily from the heavy S atom. With the increase in collision energy, the light H$_2$ product with higher internal energy can move with little or no interference from the heavy S atom and will move in the same direction as the reagent H′ atom. The exchange
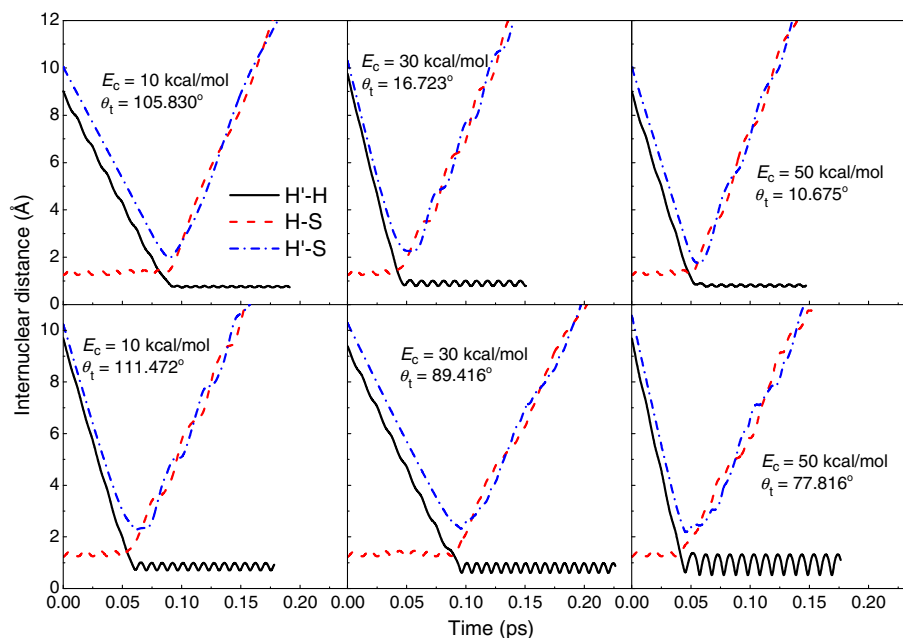
Figure 4. Internuclear distance of H′H, HS, H′S as a function of propagation time in abstraction reaction H′ + HS→H$_2$ + S.

reaction channel belongs to a light–heavy–light (LHL) mass combination. As the product H atom is light, it hardly causes any effect on the motion of the heavy product molecule H′S and the product H′S will move in the same direction of the S atom from the reagent molecule.

Figure 6 shows the $P(\theta_r)$ distribution which describes the **k**–**j**′ correlation. Three collision energies

(10, 30, 50) kcal/mol were chosen for the title reactions. From figure 6, the peaks of $P(\theta_r)$ are at θ_r angles close to 90° and are symmetric with respect to 90°, which demonstrates that the product rotational angular momentum **j**′ is distributed with cylindrical symmetry with respect to the axis perpendicular to the scattering plane (the *y*-axis) and the direction of **j**′ has a preferential alignment perpendicular to reagent initial relative
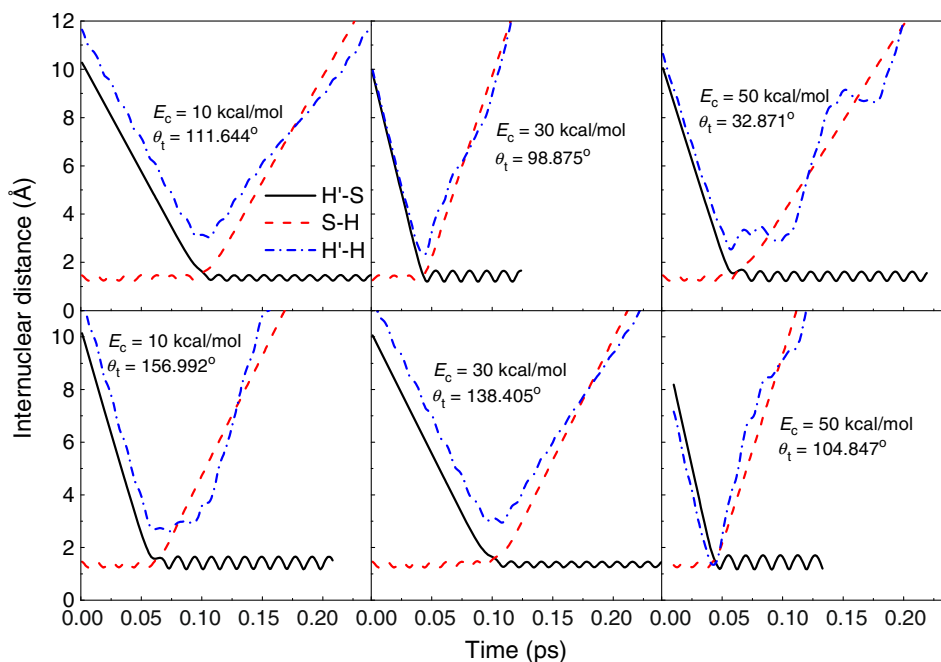

Figure 5. Internuclear distance of H′S, SH, H′H as a function of propagation time in exchange reaction H′ + HS→H + H′S.
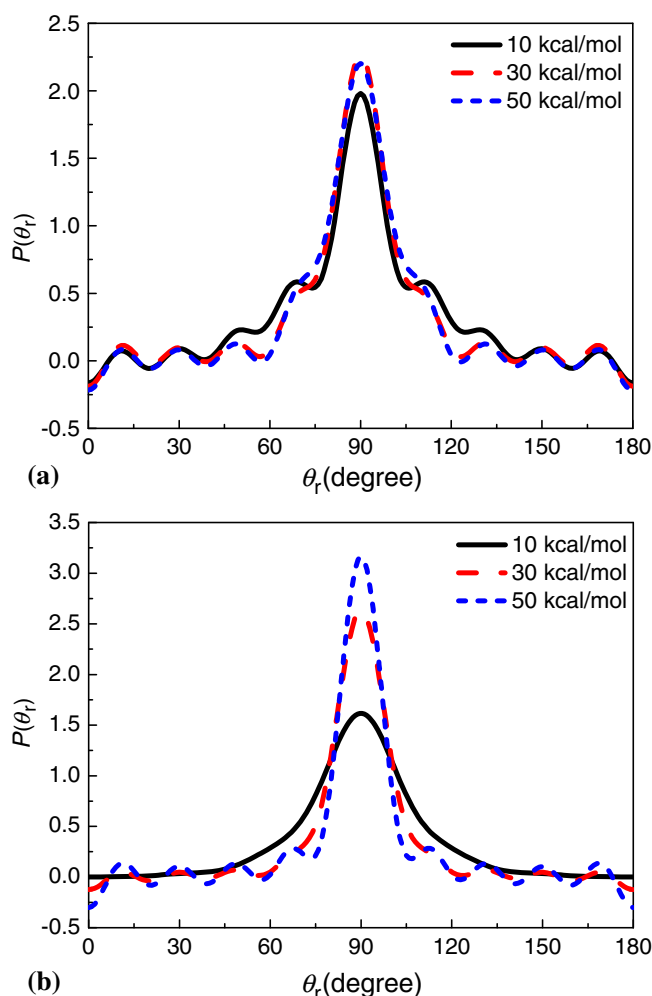
(a)

(b)

Figure 6. Angular distributions of $P(\theta_r)$, reflecting the k–j' correlation, for (**a**) the abstraction reaction H′ + HS($v =$ 0, $j = 0$)→H$_2$ + S, and (**b**) the exchange reaction H′ + HS($v = 0$, $j = 0$)→H + H′S.

velocity vector k direction. The polarization of product in abstraction reaction channel H′ + HS($v = 0$, $j = 0$)→H$_2$ + S is shown in figure 6 (a). With the increase in collision energy, the peak of $P(\theta_r)$ slightly becomes higher and narrower, which means the degree of alignment of the rotational angular momentum of the product molecules ($\vec{j'}$) with respect to $\vec{k}$ becomes stronger with the increasing collision energy. However, the peak of $P(\theta_r)$ nearly keeps constant as the collision energy rises from 30 to 50 kcal/mol. The result reflects that the alignment of product is not very sensitive to collision energy in the abstraction reaction. Figure 6 (b) shows the $P(\theta_r)$ distribution in the exchange reaction channel H′ + HS($v = 0$, $j = 0$)→H + H′S. From the figure, the peak becomes much higher and narrower with the increase in collision energy, indicating that the collision energy effectively enhances the rotational

alignment of the product. According to the refs [28, 56, 57], the distribution of $P(\theta_r)$ is related to two factors: the characteristic properties of the potential energy surface and the mass factor. The abstraction and exchange reactions are on two different pathways of the PES and the topographies of the two pathways are diverse, so it is no surprise that the alignment of j' shows differences in the two reactions.

The dihedral angular distributions of $P(\phi_r)$ for the two reactions shown in figure 6, describe k–k'–j' correlations. By comparing figure 7 (a) and (b), some similar characteristics can be found. The peaks of $P(\phi_r)$ appear at $\phi_r = 90°$ and 270°, which indicates that the j' of two kinds of product molecule are both preferentially aligned along the y-axis of CM frame. Moreover, the peaks at $\phi_r = 270°$ are much stronger than that at $\phi_r = 90°$, indicating j' is not only aligned, but also
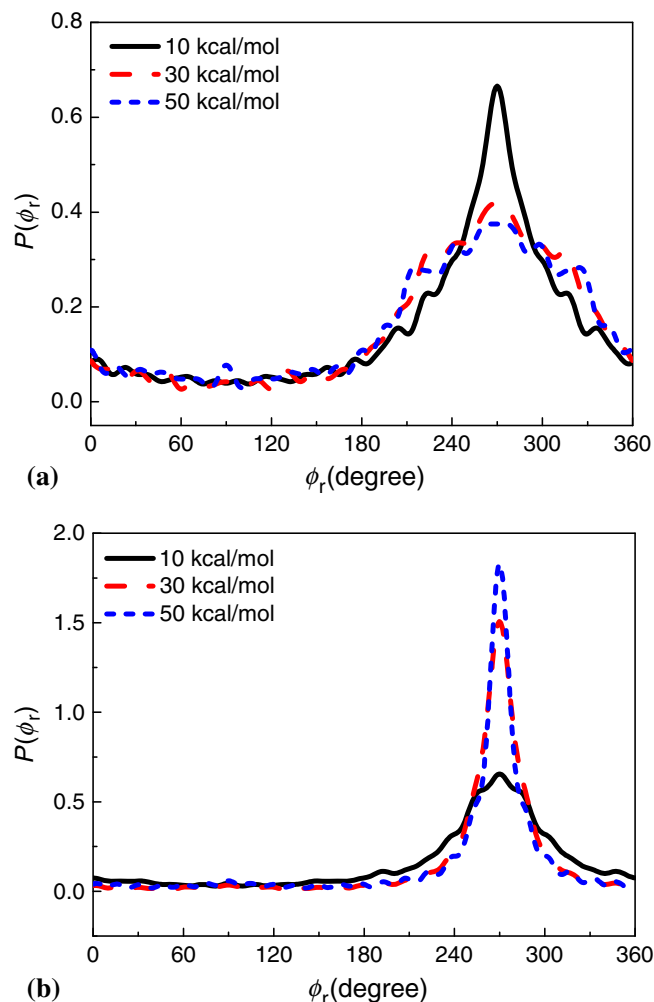

(a)

(b)

Figure 7. Angular distributions of $P(\phi_r)$, reflecting the k–k'–j' correlation, for (**a**) the abstraction reaction H′ + HS($v =$ 0, $j = 0$)→H$_2$ + S, and (**b**) the exchange reaction H′ + HS($v = 0$, $j = 0$)→H + H′S.

oriented along the negative direction of the *y*-axis, namely most of the products are scattered with clockwise rotation on the PES. It is noteworthy that the distributions of $P(\phi_r)$ are asymmetric, directly reflecting the strong polarization of j'. The 'impulsive–collision model'[58,59] of atom and molecule reaction A + BC→AB + C developed by Han *et al.* can well account for this asymmetry. The product rotational angular momentum j' can be expressed as $j' = L \sin^2 \beta + j \cos^2 \beta + J_1 m_B/m_{AB}$, where L and j are the orbital and rotational angular momentum of the reactant molecule BC, respectively. $J_1 = \sqrt{\mu_{BC} R}(r_{AB} \times r_{CB})$, with $r_{AB} = r_A - r_B$ and $r_{CB} = r_C - r_B$, being vectors from B pointing to A and C, respectively. The μ_{BC} is the reduced mass of the BC molecule and R is the repulsive energy between B and C atoms. During the chemical bond forming and breaking for the title reaction, the term $L \sin^2 \beta + j \cos^{2\beta}$ in the equation is symmetric with respect to the k–k' scattering plane, whereas the term $J_1 m_B/m_{AB}$ has a preferred direction because of the effect of the repulsive energy R, which causes the orientation of the products. However, with the increase in collision energy, the variation trends of the orientation of product rotational angular momentum j' for these two reactions are quite different. For the abstraction reaction H' + HS($v = 0$, $j = 0$)→H$_2$ + S, as shown in figure 7 (a), the peak at $\phi_r = 270°$ becomes lower and broader with the increase in collision energy, which means that the orientation of j' becomes weaker with the increase in collision energy. For the exchange reaction H' + HS($v = 0$, $j = 0$)→H + H'S as depicted in figure 7 (b), with the increase in collision energy from 10 kcal/mol to 50 kcal/mol, the peak at $\phi_r = 270°$ becomes much higher and narrower while the peak at $\phi_r = 90°$ nearly remains unchanged, which demonstrates that the orientation of j' is enhanced with the increase in collision energy. We will use the term in-plane to refer to the preference of product molecule rotating in planes parallel to the scattering plane, and the term 'out-of-plane' to refer to the preference of product molecule rotating in the planes perpendicular to the scattering plane. From figure 7 (a), the $P(\phi_r)$ distribution becomes broader with the increase in collision energy, which indicates that the product molecule rotation has a preference of changing from the 'in-plane' reaction mechanism to the 'out-of-plane' mechanism in abstraction reaction channel. However, for the exchange channel, the rotation of product molecules tends to change from the 'out-of-plane' reaction mechanism to the 'in-plane' mechanism. We are eagerly looking forward to the experimental studies of the stereodynamics for this reverse reaction, and a comparison can be conducted between theory and experiment.

4. Conclusions

In this study, we employ the QCT method to study the vector correlations between the product and reagent for reaction H' + HS($v = 0$, $j = 0$) on a newly computed ^{3}A″ PES. There are two reaction channels for H' + HS on the lowest adiabatic state H$_2$S (^{3}A″), and a dynamics study of the title reactions can provide useful information on hydrogen-atom abstraction and exchange reactions. The reaction integral/differential cross-sections and product's angular momentum polarization were calculated for collision energies ranging from 0 to 50 kcal/mol. The QCT calculated reaction integral cross-sections for these two reaction channels are in good agreement with earlier TDWP results. Both the abstraction and exchange reactions are mainly governed by direct reaction mechanism within the studied energy range. The calculated differential cross-section reveals that the collision energy has remarkably distinguishable influence on the angular distributions of products in the two reaction channels and the differences can be closely related to the different mass combination. The product rotational angular momentum j' is not only aligned perpendicular to the scattering plane but also oriented along the negative direction of the *y*-axis. For the abstraction reaction, with the increase in collision energy, the alignment of j' of the product H$_2$ becomes stronger, whereas the orientation along negative direction of the *y*-axis becomes weaker. For the exchange reaction, the degrees of alignment and orientation of j' of the product H'S, both increase with the increase in collision energy.

References

1. Chang A H H and Lin S-H 2000 *Chem. Phys. Lett.* **320** 161
2. Aoiz F J, Bañares L and Herrero V J 2006 *J. Phys. Chem.* **A110** 12546
3. Zyubin A S, Mebel A M, Chao S D and Skodje R T 2001 *J. Chem. Phys.* **114** 320
4. Ho T S, Hollebeek T, Rabitz H, Chao S D, Skodje R T, Zyubin A S and Mebel A M 2002 *J. Chem. Phys.* **116** 4124
5. Chao S-D and Skodje R T 2001 *J. Phys. Chem.* **A105** 2474

6. Bañares L, Aoiz F J, Honvault P and Launay J M 2004 *J. Phys. Chem.* **A108** 1616
7. Bañares L, Castillo J F, Honvault P and Launay J M 2005 *Phys. Chem. Chem. Phys.* **7** 627
8. Honvault P and Launay J M 2003 *Chem. Phys. Lett.* **370** 371
9. Rackham E J, González-Lezana T and Manolopoulos D E 2003 *J. Chem. Phys.* **119** 12895
10. Aoiz F J, González-Lezana T and Rábanos V S 2008 *J. Chem. Phys.* **129** 094305
11. González-Lezana T 2007 *Int. Rev. Phys. Chem.* **26** 29
12. Lin S-Y and Guo H 2005 *J. Chem. Phys.* **122** 074304
13. Klos J A, Dagdigian P J and Alexander M H 2007 *J. Chem. Phys.* **127** 154321
14. Maiti B, Schatz G C and Lendvay G 2004 *J. Phys. Chem.* **A108** 8772
15. Lee S H and Liu K 1998 *J. Phys. Chem.* **A102** 8637
16. Lee S H and Liu K 1998 *Chem. Phys. Lett.* **290** 323
17. Lee S H and Liu K 2000 In *Advances in molecular beam research and applications*, Berlin: Springer-Verlag
18. Berteloite C, Lara M, Bergeat A, Le Picard S D, Dayou F, Hickson K M, Canosa A, Naulin C, Launay J M, Sims I R and Costes M 2010 *Phys. Rev. Lett.* **105** 203201
19. Lara M, Jambrina P G, Varandas A J C, Launay J M and Aoiz F J 2011 *J. Chem. Phys.* **135** 134313
20. Chu T-S, Han K-L and Schatz G C 2007 *J. Phys. Chem.* **A111** 8286
21. Yang H, Han K-L, Schatz G C, Lee S H, Liu K, Smith S C and Hankel M 2009 *Phys. Chem. Chem. Phys.* **11** 11587
22. Rackham E J, Huarte-Larranaga F and Manolopoulos D E 2001 *Chem. Phys. Lett.* **343** 356
23. Song Y-Z and Varandas A J C 2009 *J. Chem. Phys.* **130** 134317
24. Varandas A J C 2007 *J. Chem. Phys.* **126** 244105
25. Martin R L 1983 *Chem. Phys.* **82** 337
26. Lv S-J, Zhang P-Y, Han K-L and He G-Z 2012 *J. Chem. Phys.* **136** 094308
27. Aoiz F J, Brouard M and Enriquez P A 1996 *J. Chem. Phys.* **105** 4964
28. Wang M-L, Han K-L and He G-Z 1998 *J. Chem. Phys.* **109** 5446
29. Brouard M, Lambert H M, Rayner S P and Simons J P 1996 *Mol. Phys.* **89** 403
30. Han K-L, He G-Z and Lou N-Q 1996 *J. Chem. Phys.* **105** 8699
31. Knowles P J and Werner H J 1985 *Chem. Phys. Lett.* **115** 259
32. Werner H J and Knowles P J 1985 *J. Chem. Phys.* **82** 5053
33. Knowles P J and Werner H J 1988 *Chem. Phys. Lett.* **145** 514
34. Werner H J and Knowles P J 1988 *J. Chem. Phys.* **89** 5803
35. Knowles P J and Werner H J 1992 *Theor. Chim. Acta.* **84** 95
36. Kendall R A, Dunning T H and Harrison R J 1992 *J. Chem. Phys.* **96** 6796
37. Davidson E R and Silver D W 1977 *Chem. Phys. Lett.* **52** 403
38. Aguado A and Paniagua M 1992 *J. Chem. Phys.* **96** 1265
39. Aguado A, Tablero C and Paniagua M 1998 *Comput. Phys. Commun.* **108** 259
40. Levine R D and Bernstein R B 1974 *Molecular reaction dynamics*, New York: Oxford University Press
41. Varandas A J C 1994 *Chem. Phys. Lett.* **225** 18
42. Nyman G and Wilhelmsson U 1994 *J. Chem. Phys.* **96** 5198
43. Nyman G and Davidsson J 1990 *J. Chem. Phys.* **92** 2415
44. Stock G and Muller U 1999 *J. Chem. Phys.* **111** 65
45. Muller U and Stock G 1999 *J. Chem. Phys.* **111** 77
46. Lu D-h and Hase W L 1988 *J. Chem. Phys.* **89** 6723
47. Schatz G C 1983 *J. Chem. Phys.* **79** 5386
48. Varandas A J C 2007 *Chem. Phys. Lett.* **439** 386
49. Bowman J M, Gazdy B and Sun Q 1989 *J. Chem. Phys.* **91** 2859
50. Miller W H, Hase W L and Darling C L 1989 *J. Chem. Phys.* **91** 2863
51. Czakó G and Bowman J M 2009 *J. Chem. Phys.* **131** 244302
52. Czakó G, Kaledin A L and Bowman J M 2010 *J. Chem. Phys.* **132** 164103
53. Sun Z-G, Guo H and Zhang D-H 2010 *J. Chem. Phys.* **132** 084112
54. Fu B-N and Zhang D-H 2007 *J. Chem. Phys.* **A111** 9516
55. Zhang W-Q, Zhou Y, Wu G-R, Lu Y-P, Pan H-L, Fu B-N, Shuai Q, Liu L, Liu S, Zhang L-L, Jiang B, Dai D-X, Lee S-Y, Xie Z, Braams B J, Bowman J M, Collins M A, Zhang D-H and Yang X-M 2010 *Proc. Natl. Acad. Sci. USA* **107** 12782
56. Wang M-L, Han K-L and He G-Z 1998 *J. Phys. Chem.* **A102** 10204
57. Zhao J, Xu Y and Meng Q-T 2009 *J. Phys.* **B42** 165006
58. Li R-J, Han K-L, Li F-E, Lu R-C, He G-Z and Lou N-Q 1994 *Chem. Phys. Lett.* **220** 281
59. Han K-L, Zhang L, Xu D-L, He G-Z and Lou N-Q 2001 *J. Phys. Chem.* **A105** 2956